Progress In Electromagnetics Research, Vol. 150, 49–57, 2015

Spatially Mapped Metamaterials Make a New Magnetic Concentrator for the Two-Coil System

Yingyi Zhang*, Chen Yao, Houjun Tang, and Yuncheng Li

Abstract—Magnetic lens based on metamaterials has helped to increase the inductive coupling of two-coil system in wireless power transfer. By coordinate transformation, the spatially mapped metamaterials are proposed in this paper for a new magnetic concentrator in two-coil system to improve the mutual coupling. To achieve such metamaterials, the virtual rectangular domain is spatially mapped into a deformed spherical shell. The effects of such mapped spherical shell, functioning as magnetic concentrator, are simulated and evaluated. The fabrication and simplification of this magnetic concentrator are also considered. Finally, this model of spherical shell is compared with that of a traditional magnetic concentrator to demonstrate its advantage.

1. INTRODUCTION

In the last few years, two-coil systems working at megahertz for wireless power transfer (WPT) have become standard in implanted biomedical devices [1], telemetry systems [2] and sensor arrays [3]. In these applications, the energy transferred is confined within a short range because of a rapid decay in the inductive coupling from a diverging magnetic field between transmitting and receiving coils. To improve the inductive coupling in these two-coil systems, metamaterials based on the concept of the "perfect lens" [4] were introduced. Metamaterials are artificial materials which are manufactured according to a specific structure and possess anisotropic distributed properties not present in nature. Theoretical analysis [5], numerical simulation [6], and experimental verification [7] on finite slabs made of metamaterial have demonstrated enhancements in inductive coupling of the two-coil systems.

Compared with conditions of perfect imaging in optics, there are no strict conditions imposed on two-coil systems with metamaterials. Hence, the position and shape of slabs can be adjusted to optimize magnetic coupling and space utilization [8]. Previous experimental results [9] indicate that the mutual coupling of entire system is still enhanced with metamaterials close to a receiving coil. Actually, the metamaterials in some situations do need to be close to the receiving coil for better energy harvest [10]. In this paper, the spatially mapped metamaterials are proposed to make a magnetic concentrator surrounding the receiving coil. By mapping the virtual domain to spherical shell, the magnetic field is equivalently mapped to a deformed domain to increase the inductive coupling of two-coil system.

The previous studies on metamaterials in a two-coil system were limited to the periodic structures [11] that exhibited only isotropic and homogeneous properties. The spatially mapped metamaterials derived from the coordinate transformation showed anisotropic and inhomogeneous characteristics that enable electromagnetic (EM) fields to be flexibly manipulated [12]. The coordinate transformation method was applied to form devices such as invisible cloak [13], microwave rotator [14], and electromagnetic concentrator [15], where the transformed domain was not deformed. This paper analyzes the magnetic performance of these metamaterials. Even if the boundary after transformation is discontinuous, enhancements on the mutual inductance can still be achieved. Finally, the results are

Received 1 November 2014, Accepted 15 December 2014, Scheduled 21 December 2014

* Corresponding author: Yingyi Zhang (zhangyingyi@sjtu.edu.cn).

The authors are with the Key Laboratory of Control of Power Transmission and Transformation Ministry of Education, Shanghai Jiao Tong University, 800 Dongchuan RD., Shanghai 200240, China.

compared with those from a traditional electromagnetic concentrator [15] to benchmark the performance enhancement.

2. ANALYSIS OF COORDINATE TRANSFORMATION

Based on the form invariance of Maxwell's equations, the coordinate transformation can manipulate the EM field by altering the EM tensors. Supposing time invariance for the coordinate transformation, the viable form of the permittivity and permeability tensors derived from Maxwell's equations are written [16];

$$\begin{aligned} \varepsilon^{i'j'} &= \left[\det\left(A_i^{i'}\right)\right]^{-1} A_i^{i'} A_j^{j'} \varepsilon^{ij} \\ \mu^{i'j'} &= \left[\det\left(A_i^{i'}\right)\right]^{-1} A_i^{i'} A_j^{j'} \mu^{ij}. \end{aligned} \tag{1}$$

Here A denotes the Jacobi transformation matrix, and Eq. (1) defines bases for designing spatially mapped metamaterials. Even if we only use partial properties of the coordinate transformation compared with that for a strict invisible cloak or a concentrator, the effects of magnetic concentrator made of such metamaterials still hold.

To design a new magnetic concentrator so as to increase the effective flux passing through the receiving coil in the WPT system, spatially mapped metamaterials are designed in the form of spherical shells enclosing the receiving coils (see Fig. 1). The inner radius of the shell is denoted R and its thickness t. The virtual rectangular domain, outlined by a dash line, represents the original space of the mapped spherical shell. Its thickness is denoted T. The distance between the center of the shell and the virtual domain is d. Using the coordinate transformation, the virtual domain is linearly mapped into the spherical shell domain. Here, we establish a spherical coordinate system with origin at the center of spherical shell. Suppose point $P(r, \theta, \varphi)$ is in the unmapped rectangular domain. The angle between the vector with endpoint $P(r, \theta, \varphi)$ and the z-axis is θ and the corresponding point in the spherical domain is $P(r', \theta', \varphi')$. The transformation for the spatial mapping can be written in component form as

$$\begin{aligned} r' &= (r\cos\theta - d)t/T + R \\ \theta' &= \theta \\ \varphi' &= \varphi \end{aligned} \tag{2}$$

As evident in Fig. 1, Eq. (2) involves two geometric transformations: the rectangular domain of thickness T being compressed into a narrow space of thickness t and the compressed narrow space then being bent into a spherical shell of inner radius R. The divergent magnetic flux in the original virtual space is bent into the spherical shell under spatial mapping (see Fig. 2(a)). With the presence of the

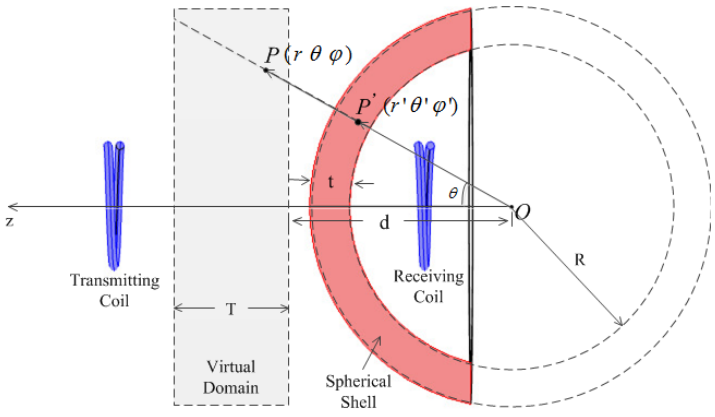

Figure 1. Magnetic concentrator produced under a spatial mapping transformation.

mapped spherical shell, the magnetic field distribution is more convergent and closer to the receiving coil; this proximity, as magnetic concentrator, helps to increase the flux and mutual coupling of two-coil system.

The Jacobi transformation matrix can be derived from Eq. (2) according to the transformation optics in orthogonal coordinate [17]. Considering scaling factor in spherical coordinate, the A matrix is written;

$$A = \begin{bmatrix} \frac{h_{r'}}{h_r}\frac{\partial r'}{\partial r} & \frac{h_{r'}}{h_\theta}\frac{\partial r'}{\partial \theta} & \frac{h_{r'}}{h_\varphi}\frac{\partial r'}{\partial \varphi} \\ \frac{h_{\theta'}}{h_r}\frac{\partial \theta'}{\partial r} & \frac{h_{\theta'}}{h_\theta}\frac{\partial \theta'}{\partial \theta} & \frac{h_{\theta'}}{h_\varphi}\frac{\partial \theta'}{\partial \varphi} \\ \frac{h_{\varphi'}}{h_r}\frac{\partial \varphi'}{\partial r} & \frac{h_{\varphi'}}{h_\theta}\frac{\partial \varphi'}{\partial \theta} & \frac{h_{\varphi'}}{h_\varphi}\frac{\partial \varphi'}{\partial \varphi} \end{bmatrix} = \begin{bmatrix} \frac{t}{T}\cos\theta & -\frac{t}{T}\sin\theta & 0 \\ 0 & \frac{r'}{r} & 0 \\ 0 & 0 & \frac{r'}{r} \end{bmatrix} \tag{3}$$

Using Jacobi matrix, the permittivity and permeability tensors can be deduced by the inverse of Eq. (1), specifically $r = ((r' - R)T/t + d)/\cos\theta$, to replace the component r in the final matrix.

$$\varepsilon_r^{(r',\theta',\varphi')}, \mu_r^{(r',\theta',\varphi')} = \begin{bmatrix} a^2 b(1/\cos\theta') & -a\tan\theta' & 0 \\ -a\tan\theta' & 1/(b\cos\theta') & 0 \\ 0 & 0 & 1/(b\cos\theta') \end{bmatrix}. \tag{4}$$

Here $a = (r' - R)T/(tr'\cos\theta') + d/(r'\cos\theta')$ and $b = t/T$. In the material interpretation, the transformation Eq. (2) is incomplete because the compression transformation in the space $r' < R$ and the extension transformation in the space $r' > R + t$ are both undefined. However, considering the practical demands in two-coil systems, these spaces are assumed to be air-filled, available for the placement of the transmitting and receiving coils.

To give an intuitive exhibition of bending EM field by spatial mapping, the spherical shell under 2D view is simulated in different cases. In Figs. 2(b), (c), the plane wave and line source (perpendicular to

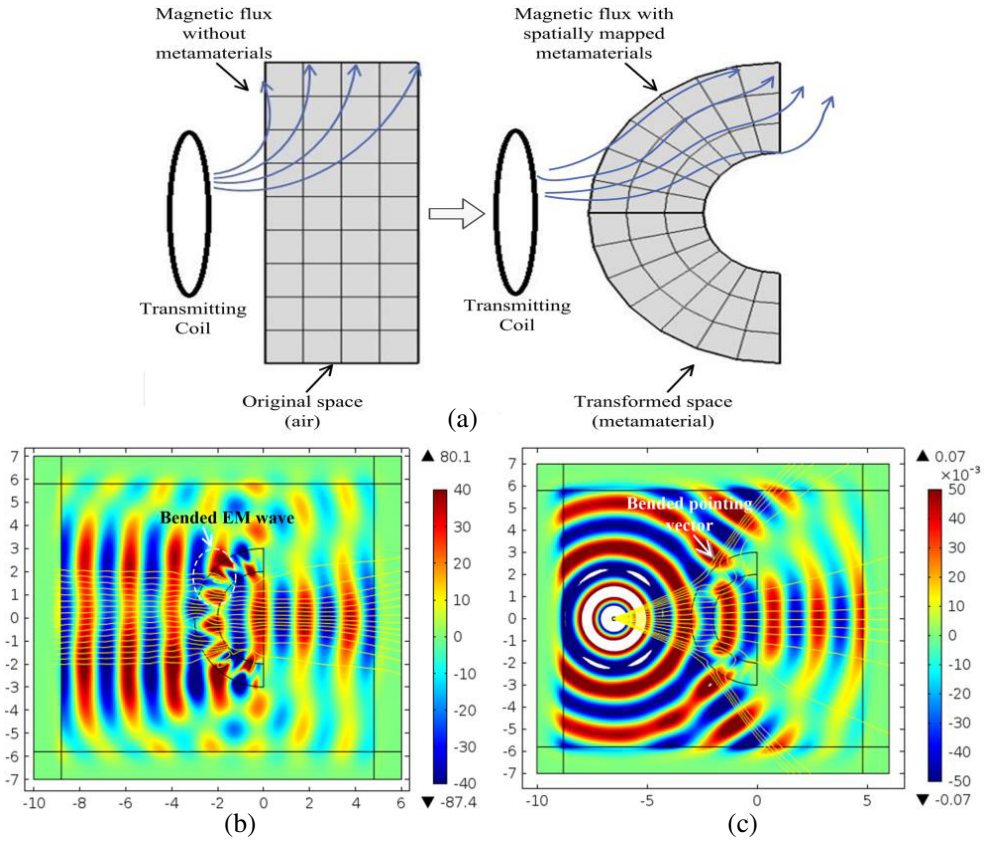

Figure 2. (a) Bending magnetic flux using a spatially mapped metamaterial. Bending EM wave and pointing vector by metamaterial shell (b) with incident plane wave. (c) With electric line source.

the plane) are selected as the excitation respectively. The entire model is designed based on Eq. (4) and evaluated in terms of EM field and pointing vector at radio frequency (15 GHz). As displayed in both figures, the distribution of transmitted EM wave is relatively extruded and the pointing vector lines is obviously bended. Previous work [12] indicated that the coordinate transformation can be applied at all frequencies from optical down to DC, so the metamaterial shell based on spatial mapping is also considered to make the magnetic field bended and more convergent in near-field situation, especially in the two-coil system at megahertz. Hence, in the following section, a two-coil simulation model is established to verify the effects of the magnetic concentrator made of spatially mapped metamaterials.

3. SIMULATION OF MAGNETIC CONCENTRATOR IN TWO-COIL SYSTEM

A two-coil system with concentrator is depicted in Fig. 3(a) in the 3D COMSOL solver. Two single-turn coils of 15-cm radius are placed 80 cm apart. The left coil is the transmitting coil excited by 1 MHz, 10 A alternative current. The receiving coil is partially encircled by a magnetic concentrator (spherical shell) of 50-cm radius and 10-cm thickness. A huge sphere with a 240-cm-radius, 10-cm-thick, perfectly matched layer is established as the solving domain. A 1-kΩ load resistor and proper compensating capacitors are also connected to the receiving coil for a more practical evaluation. A 2D schematic of the entire system (including power source, coils and load) is given in Fig. 3(b).

At first, the two-coil system with no metamaterials is simulated; the distribution of the flux density B is displayed in Fig. 4(a). The spherical shell is assumed filled with air for this simulation. In Fig. 4, the color scale indicates the value of flux density. The magnetic field in Fig. 4(a) diverges quickly near the transmitting coil, and the flux densities near the receiving coil fall in the range between 1.95e-7 and 2.08e-7 T. Clearly, the effective flux through the receiving coil is very limited. By numerical computation, the mutual inductance of the transmitting and receiving coils is only 6.8 nH, and the power measured at load is only 0.69 mW, indicating weak mutual coupling of the two-coil system.

Next, the magnetic concentrator with spatially mapped metamaterials is added into the system. The tensor components for permittivity and permeability are computed using Eq. (4) and expressed in spherical coordinates with the origin at the center of the spherical shell. Assuming thickness $T = t$ for the virtual domain and varying distance d from 20 cm to 80 cm in 10-cm step, changes in the distribution of the flux density B appear near the receiving coil (see Figs. 4(b)–(d)).

By the coordinate transformation, the rectangular domain is mapped into a spherical shell with flux density bent inside the shell [Fig. 4(b)]. Flux density values are higher in the receiving coil than for the system with nothing. That is, the effective flux has increased thereby improving the mutual coupling. Additionally, from Figs. 4 (b)–(d), we can conclude that by increasing distance between virtual domain and spherical shell, flux density near the receiving coil becomes stronger. That is because the fact that the virtual domain to be mapped is approaching the transmitting coil where the flux density is stronger.

In a further numerical analysis, the power is measured at load, and the mutual inductance is

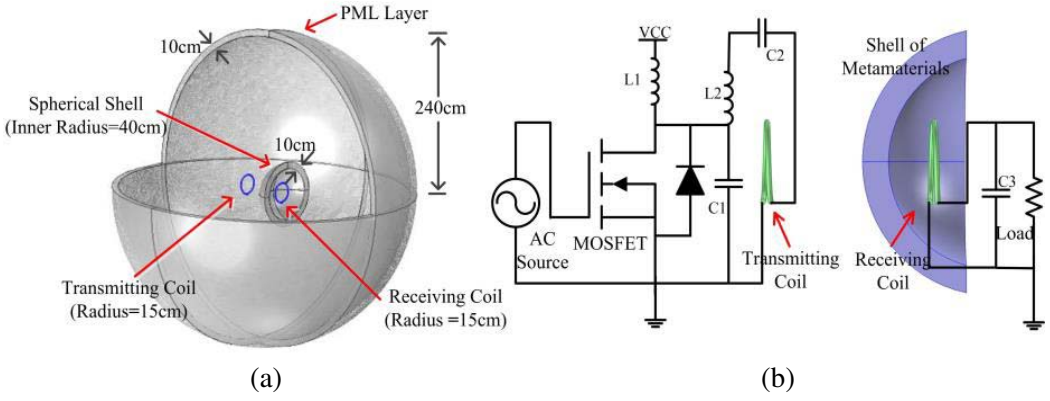

Figure 3. (a) Two-coil system in 3D view. (b) Side view of the two-coil system with concentrator.

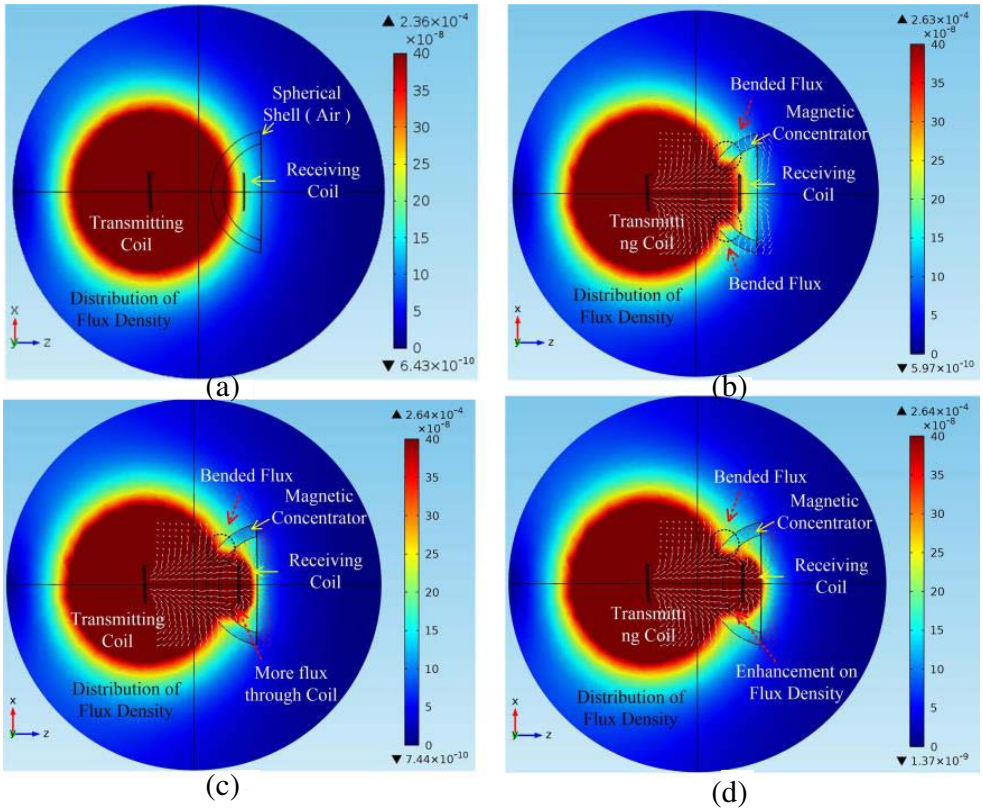

Figure 4. Distribution of flux density. (a) Without concentrator. (b) With concentrator and $d = 20\,\text{cm}$. (c) With concentrator and $d = 50\,\text{cm}$. (d) With concentrator and $d = 80\,\text{cm}$.

computed by $M = \iint \vec{B}_z \cdot d\vec{s}/I$. The data results are plotted in Fig. 5. The mutual inductance is an indicator and the dominant factor of coupling intensity of two-coil WPT system. The higher mutual inductance is, the less flux leakage and the more inductive energy derived from the flux are obtained at the receiving coil. Hence, the mutual inductance directly affects the power transferred to the load and the mutual coupling of the system; this is partly seen from the trend in the blue line in Figs. 5(a) and (b). Apparently, with metamaterials concentrator, both mutual inductance and power at load are enhanced. Moreover, longer distances can be achieved if the mutual inductance does not change in the original system.

4. FABRICATION CONSIDERATION OF MAGNETIC CONCENTRATOR

Although the performance of magnetic concentrator is good, the permeability tensor of the metamaterial is quite complicated. With practical applications and possible fabrication in mind, the parameters determining the tensor should be partly simplified. (All cases are simulated with $d = 40\,\text{cm}$.)

To begin, the current EM parameter varies with radius continuously. To simplify it, we segment the concentrator shell into multiple layers and fix the value of the parameter in each layer. For example, we segmented the shell into five layers, and parameter r' is set to 49 cm, 47 cm, 45 cm, 43 cm, and 41 cm. With other parameters unaltered, the flux density is depicted in Fig. 6(a) with the corresponding mutual inductance displayed in green in Fig. 5(b). The result for the multiple-layered metamaterials agrees well with a previous result. Obviously, a shell segmented into finer layers will yield a better approximation.

Secondly, the electromagnetic tensor for metamaterials with a multilayered structure is still anisotropic. Here we reduce the EM parameter in the tensor artificially by setting the non-diagonal element $-a \tan\theta'$ to zero. Up till now, the EM tensor has been a diagonal matrix, which means that the material is uniaxial and fabrication practicable. By numerical analysis, the flux density is

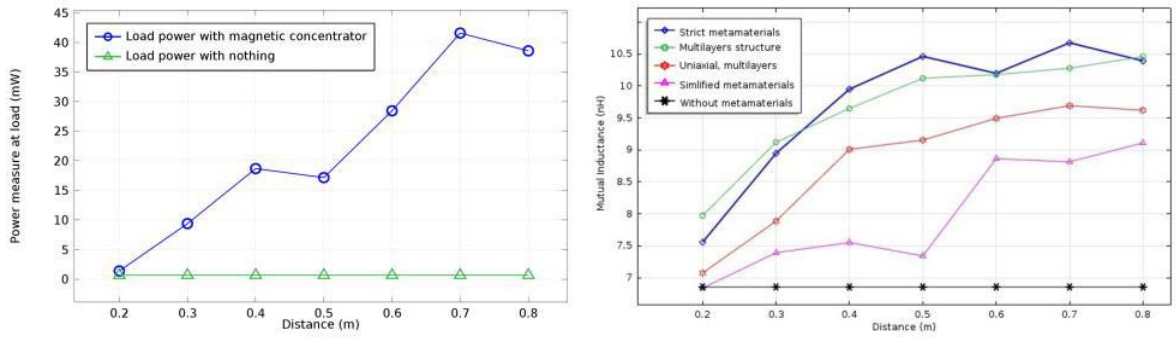

Figure 5. (a) Power measured at load with and without concentrator. (b) Mutual inductance of two coils under different structural types (including strict metamaterials, metamaterials with multilayers structures, uniaxial metamaterials with multilayers structure, simplified metamaterials, and without metamaterials).

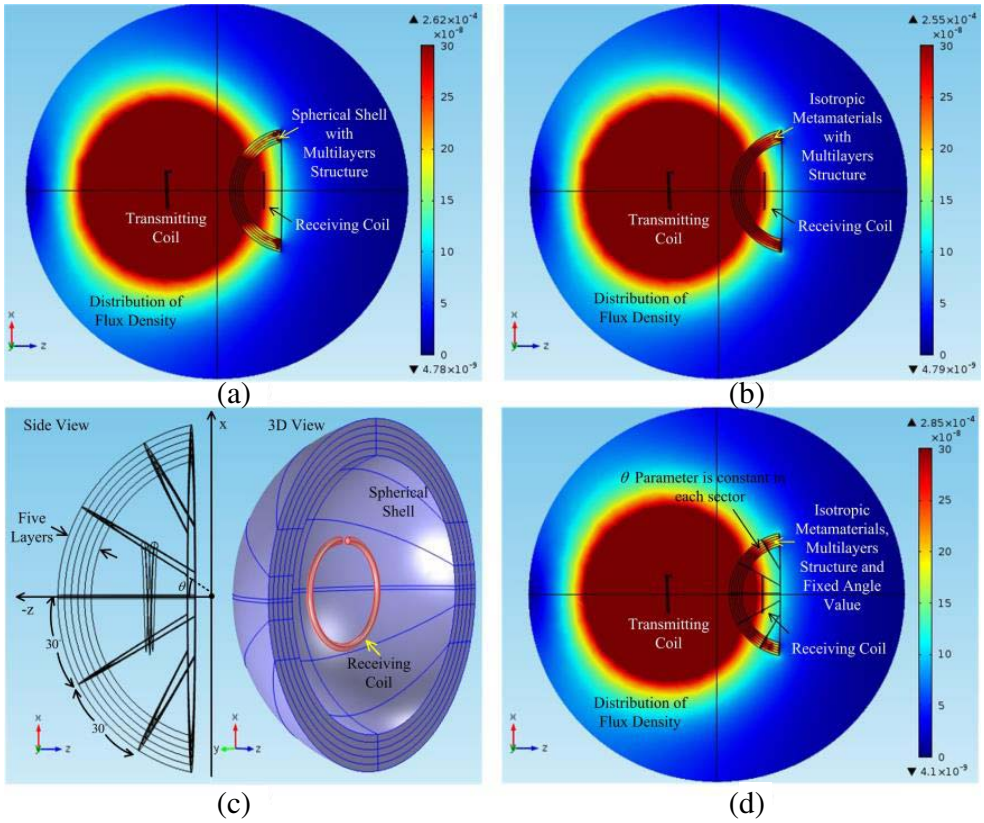

Figure 6. (a) Flux density of concentrator with multilayers structure. (b) Flux density of concentrator with diagonal EM tensor (uniaxial) and multilayers structure. (c) Schematics of a magnetic concentrator segmented into five layers and six sectors. (d) Flux density of the concentrator of uniaxial metamaterials with multi-sectored structure and a fixed angle value in each sector.

displayed in Fig. 6(b); the mutual inductance of the system with uniaxial metamaterials is displayed in red in Fig. 5(b). Although the performance of magnetic concentrator of uniaxial materials with multilayers begins to decrease, the mutual inductance is still fairly enhanced compared with that without metamaterials.

Finally, for the angular dependence of the EM parameter, we divide the range of angle θ' into several sectors. In each sector, the EM parameter is set to a fixed value. For simplicity, we opt for six sectors symmetrically arranged with three different angle ranges: $0^\circ \sim 30^\circ$, $30^\circ \sim 60^\circ$, and $60^\circ \sim 75^\circ$ (see Fig. 6(c)); in each sector, the value of θ' is set to 15°, 45° and 65° respectively. The EM parameter in each sector of each layer is now constant and the entire tensor is diagonal, making fabrication possible. Specifically, isotropic material can be achieved in special case where $\theta' = 0^\circ$. The flux density of magnetic concentrator of uniaxial metamaterials with fixed angle values and multilayered structure is displayed in Fig. 6(d).

For convenience, we refer to such metamaterials as simplified metamaterials. The mutual inductance of the system with simplified metamaterial is depicted in magenta in Fig. 5(b). From a comparison between Figs. 5 and 6, we conclude that, with the concentrator of simplified metamaterials, the performance is still better than the systems with nothing. The most significant point is that we can fabricate such magnetic concentrator employing radial and angular multilayered structures of uniaxial materials.

5. COMPARISON WITH TRADITIONAL EM CONCENTRATOR

The electromagnetic concentrator was proposed for applications requiring electromagnetic fields to be localized [16]. Distinct from spatial mapping transformation, the EM concentrator required different transformations over different regions. Here we consider a typical three-concentric-sphere concentrator with radii $R1, R2$, and $R3$. The equations for the concentrators are written;

$$\begin{aligned} r' &= \begin{cases} \dfrac{R1}{R2} r & 0 \le r \le R2 \\ \dfrac{R3 - R1}{R3 - R2} r - \dfrac{R2 - R1}{R3 - R2} R3 & R2 < r < R3 \end{cases} \\ \theta' &= \theta \\ \varphi' &= \varphi \end{aligned} \tag{5}$$

Here, the space in $0 \le r \le R2$ is compressed into the region $0 \le r \le R1$ and the space in $R2 \le r \le R3$ expanded into region $R1 < r \le R3$. For further analysis, a model of the concentrator is configured with $R1 = 30\,\text{cm}$, $R2 = 40\,\text{cm}$, and $R3 = 50\,\text{cm}$. Other parameter settings are the same as those in the spatially-mapped-metamaterial concentrator. The flux density B was displayed in Fig. 7 with the same scale.

The flux density reveals the concentration of the magnetic field. The effective flux has increased, however, at the expense of transforming more space. That is, if a higher flux density or energy density is required, an increasing size of the anisotropic metamaterials is needed. The mutual inductance with the EM concentrator is 0.71 nH. In the light of aforementioned discussion, the mutual inductance M in the two-coil system with the different structures can be ranked as follows:

M with spatially mapped metamaterial $>M$ with EM concentrator $>M$ without metamaterial.

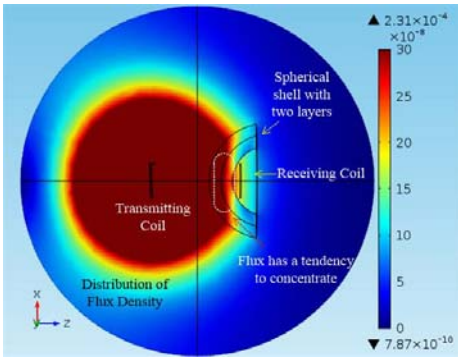

Figure 7. Flux density of traditional EM concentrator.

The disadvantage of traditional EM concentrator is two-fold: more space is required if more flux concentration is desired, and the inner sphere region needs filling with metamaterial, which is impractical for placing receiving coil. There are no such limitations in the spatially-mapped magnetic concentrator because the region inside the spherical shell is air-filled. Additionally, greater flux density in the receiving coil can be achieved by increasing distance d between virtual domain and spherical shell.

6. CONCLUSION

Spatially mapped metamaterials are proposed in this paper to make a new magnetic concentrator. Their performance in the two-coil system is numerically analyzed to verify the mutual coupling enhancement. For both flux density and mutual inductance, the results of such WPT systems are better than systems without concentrator. Using the spatial mapping transformation, more flux density and power in the receiving coil can be achieved by increasing the virtual domain distance. From the perspective of practical applications, flux density and mutual inductance of the simplified metamaterials are proved to be satisfied. These simplified metamaterials with radial and angular multilayered structures are more practicable to fabricate and yield performances that are still better than the original system. In a comparison with a traditional EM concentrator, the magnetic concentrator with spatially mapped metamaterials occupies smaller space and achieves higher mutual inductance. The inner space of the spherical shell is air-filled, enabling the unrestricted placement of receiving coil or other devices.

ACKNOWLEDGMENT

Project Supported by the National Natural Science Foundation of China (51277120).

REFERENCES

1. RamRakhyani, A. K., S. Mirabbasi, and M. Chiao, "Design and optimization of resonance-based efficient wireless power delivery systems for biomedical implants," *IEEE Trans. Biomed. Circuits System.*, Vol. 5, No. 1, 48–63, 2011.
2. Zhu, N., R. W. Ziolkowski, and H. Xin, "A metamaterial-inspired, electrically small rectenna for high-efficiency, low power harvesting and scavenging at the global positioning system $L1$ frequency," *Appl. Phys. Lett.*, Vol. 99, 114101, 2011.
3. Rindorf, L., L. Lading, and O. Breinbjerg, "Resonantly coupled antennas for passive sensors," *Proc. IEEE Sens.*, 1611–1614, 2008.
4. Pendry, J. B., "Negative refraction makes a perfect lens," *Physical Review Letters*, Vol. 85, No. 18, 3966–3969, 2000.
5. Huang, D., Y. Urzhumov, et al., "Magnetic superlens-enhanced inductive coupling for wireless power transfer," arXiv:1204.0231v1, 2012.
6. Wang, B., T. Nishino, and K. H. Teo, "Wireless power transmission efficiency enhancement with metamaterials," *2010 IEEE International Conference on Wireless Information Technology and Systems (ICWITS)*, 1–4, IEEE, 2010.
7. Wang, B., K. H. Teo, T. Nishino, et al., "Experiments on wireless power transfer with metamaterials," *Applied Physics Letters*, Vol. 98, No. 25, 254101, 2011.
8. Wang, B. and K. H. Teo, "Wireless power transfer: Metamaterials and array of coupled resonators," *Proceedings of the IEEE*, Vol. 101, No. 6, 1359–1368, 2013.
9. Rajagopalan, A. and A. K. RamRakhyani, "Improving power transfer efficiency of a short-range telemetry system using compact metamaterials," *IEEE Transaction on Microwave Theory and Technique*, Vol. 62, No. 4, 947–955, 2014.
10. Ramahi, O. M., T. S. Almonee, et al, "Metamaterial particles for electromagnetic energy harvesting," *Applied Physics Letters*, Vol. 101, 173903, 2012.

11. Bilotti, F., A. Toscano, and L. Vegni, "Design of spiral and multiple split-ring resonators for the realization of miniaturized metamaterial samples," *IEEE Trans. Antennas Propag.*, Vol. 55, No. 8, 2258–2267, 2007.
12. Pendry, J. B., D. Schurig, and D. R. Smith, "Controlling electromagnetic fields," *Science*, Vol. 312, 1780, 2006.
13. Cummer, S. A., B. I. Popa, D. Schurig, D. R. Smith, and J. B. Pendry, "Full-wave simulations of electromagnetic cloaking structures," *Phys. Rev. E*, Vol. 74, 036621, 2006.
14. Chen, H. and C. T. Chan, "Transformation media that rotate electromagnetic fields," *Appl. Phys. Lett.*, Vol. 90, 241105, 2007.
15. Jiang, W. X., T. J. Cui, Q. Cheng, J. Y. Chin, X. M. Yang, and R. Liu, "Design of arbitrarily shaped concentrators based on conformally optical transformation of nonuniform rational B-spline surfaces," *Appl. Phys. Lett.*, Vol. 92, 264101, 2008.
16. Rahm, M., D. Schurig, D. Roberts, S. A. Cummer, D. R. Smith, and J. B. Pendry, "Design of electromagnetic cloaks and concentrators using form-invariant coordinate transformations of Maxwell's equations," *Photo. Nano. Fund. Appl.*, Vol. 6, 87, 2008.
17. Chen, H., "Transformation optics in orthogonal coordinates," *J. Opt. A: Pure Appl. Opt.*, Vol. 11, 075102, 2009.